Nanofiltration and Reverse osmosis surface topographical heterogeneities: do they matter for initial bacterial adhesion?

Ashley Allen[a], Andrea J.C. Semião[b], Olivier Habimana[a], Rory Heffernan[a], Ashkan Safari[a], Eoin Casey[a]*

[a]School of Chemical and Bioprocess Engineering, University College Dublin (UCD), Belfield, Dublin 4, IRELAND

[b]School of Engineering, University of Edinburgh, Edinburgh EH9 3JL, U.K.

*****Corresponding author: Phone: +353 1 716 1877, Email: eoin.casey@ucd.ie

Abstract

The role of the physicochemical and surface properties of NF/RO membranes influencing bacterial adhesion has been widely studied. However, there exists a poor understanding of the potential role membrane topographical heterogeneities can have on bacterial adhesion. Heterogeneities on material surfaces have been shown to influence bacterial adhesion and biofilm development. The purpose of this study was therefore to investigate whether the presence of membrane topographical heterogeneities had a significant role during bacterial adhesion as this could significantly impact on how biofouling develops on membranes during NF/RO operation. An extensive study was devised in which surface topographical heterogeneities from two commercial membranes, NF270 and BW30, were assessed for their role in the adhesion of two model organisms of different geometrical shapes, *Pseudomonas fluorescens* and *Staphylococcus epidermidis*. The influence of cross-flow velocity and permeate flux was also tested, as well as the angle to which bacteria adhered compared to the flow direction. Bacterial adhesion onto the membranes and in their surface topographical heterogeneities was assessed using Scanning Electron Microscopy (SEM), Atomic Force Microscopy (AFM), fluorescence microscopy and image analysis. Results showed that up to 30% of total adhered cells were found in membrane defect areas when defect areas only covered up to 13% of the membrane surface area. This suggests that topographical heterogeneities may play a significant role in establishing environmental niches during the early stages of biofilm development. Furthermore, no noticeable difference between the angle of cell attachment in defect areas compared to the rest of the membrane surface was found.

Keywords: topography, biofouling, nanofiltration, reverse osmosis, AFM

1. Introduction

The removal of trace contaminants and organic matter by nanofiltration (NF) and reverse osmosis (RO) processes from wastewater and surface water has become an important step in providing clean potable water [1-3]. However, bacteria adhere to the membrane surface eventually forming a biofouling layer [2, 4, 5]. Biofilm formation on membranes has a significant negative effect on process performance through permeate flux decline, loss of retention and increased pressure loss over the membrane elements [6-8]. Biofilm removal requires extensive chemical cleaning which is disruptive to the process, may cause damage to the membrane and prevent a full recovery of membrane flux and retention [9]. This in turn can lead to a financial burden, usually in the form of processing costs associated with greater energy consumption, the replacement of defective filtration units and costs pertaining to halting processes for non-routine cleaning procedures.

Similarly to other substrata, biofilm formation is prompted by the initial adhesion and subsequent consolidation of microorganisms onto membrane surfaces [10, 11]. It is therefore important to identify the different factors involved in the initial bacterial adhesion onto NF and RO membranes as this would help develop novel antifouling membrane surfaces and cleaning strategies for sustaining membrane performance. Bacterial adhesion has been found to be influenced by the surface properties of membranes such as surface charge [12-14], hydrophobicity and surface roughness [15, 16], as well as bacterial cell wall physico-chemical properties and structure [17]. Surface roughness is a parameter used to evaluate the surface topography of membranes indicating heterogeneous nano-scale peak protuberances and depressions on the membrane surface [15, 18, 19]. Analyses suggest that these nanoscale heterogeneities provide favourable binding sites for bacteria to deposit and accumulate [10, 20].

The use of surface roughness as a parameter is usually quantified as the average roughness and root mean squared roughness. However, quantifying membrane topography in the presence of surface topographical heterogeneities (redefined as surface defects throughout this study) can be challenging [21], since these are usually in the order of several micrometres in width and depth. As such, defects can be easily overlooked and excluded during AFM studies, in which scanning raster areas are usually performed at random small areas at a time [15, 18]. The presence of large surface defects on NF and RO membranes are areas larger than those featured in the minimum value of surface roughness presenting areas with lower shear rate. Microscale surface defects on other types of surfaces, such as stainless steel [22, 23] have been found to influence bacterial adhesion [24-27]. Moreover, a previous study has demonstrated preferential bacterial adhesion to substrates comprised of surface topographical heterogeneities compared to flat surfaces [28]. The analysis of bacterial adhesive behaviour to various structured surfaces has provided insights into preferential sites with high likelihood of cell adhesion and proliferation as previously demonstrated by Hou et al. [29]: the presence of micro-topographic confining features larger than 20 µm x 20 µm on structured PDMS was shown to promote the adhesion and subsequent enhanced biofilm formation of *Escherichia coli* cells.

While surface defects can promote preferential surface colonization, the size and shape of bacterial cells also need to be considered. One previous study conducted by Medilanski et al. [25], demonstrated that cell morphology influenced the cell's proficiency to adhere within surface topographical heterogeneities in the form of scratches on stainless steel created at the width of the the bacterial cells. More specifically larger *Rhodococcus* sp. showed a maximum percentage cell adhesion alignment with topographical heterogeneities of up to 7% while smaller *Pseudomonas aeruginosa* cells showed an alignment of up to 44%.

Although, the surfaces of NF and RO membranes are composed of micrometre scale surface defects, it is still unclear whether these influence the initial bacterial adhesion under full scale filtration processes. The consequence of these pronounced surface defects on membranes should not be neglected since it is unclear how these might contribute to the rate of bacterial adhesion and potentially the characteristics of the subsequent biofilm. This work provides a framework by which novel membranes with deliberate micro-topographical modification [25, 27, 28, 30-32], can be assessed from the point of view of early stage biofouling.

The aim of this study was to determine how surface defects, present on the surface of NF and RO membranes, influence bacterial adhesion, in its most basic form. In this study, two bacterial species of different morphologies, *Ps. fluorescens* and *S. epidermidis* commonly found in NF and RO biofilms during water treatment [26, 33-36] were used to test their proficiency to adhere onto micrometre scale surface defects areas of two commercial NF and RO membranes, NF270 and BW30, respectively, under flux and no-flux conditions. Additionally, the angular orientation of adhered cells in relation to flow direction was assessed to determine whether the orientation of bacteria during adhesion was influenced by flow hydrodynamics or whether it follows a stochastic process.

2. Materials and Methods

2.1. Bacterial strains, culture conditions and preparation

One Gram-negative *Pseudomonas fluorescens* PLC1701 and one Gram-positive *Staphylococcus epidermidis* ATCC 12228 model strains were selected for bacterial adhesion assays in this study. *Ps. fluorescens* is a rod-shaped bacterium with approximately 1 µm in width and 2 µm of length

and *S. epidermidis* is a cocci bacterium with approximately 1 µm of diameter. An mCherry-expressing *Ps. fluorescens* [11] was stored at -80°C in King B broth [37] supplemented with 20% glycerol. Independent *Ps. fluorescens* cultures were obtained by inoculating 100 mL King B broth supplemented with gentamicin (Sigma Aldrich, Ireland) at a final concentration of 10 µg.mL^{-1}, using a single colony of a previously grown culture on King B agar (Sigma Aldrich, Ireland) at 28°C. Independent *S. epidermidis* cultures were obtained by inoculating 100 mL Tryptic Soy Broth (TSB) using a single colony of a previously grown culture on King B agar (Sigma Aldrich, Ireland) at 28°C. Both inoculated medium were then incubated at 30°C with shaking at 75 rpm for 16 hours until the cell culture reached an optical density (OD) between 0.8-1.2 at OD_{600}. Cultures were centrifuged (eppendorf Centrifuge 5415C) at 7000 RPM for 10 min, after which the supernatant was discarded and the bacterial pellet re-suspended in Raw Water Medium without carbon (RW^{-C}), as previously described by Semião et al. [16]. Water used in preparation of the RW^{-C} was Grade 1 pure water, referred to as MilliQ water (Biopure 15 and Purelab flex 2, Veolia, Ireland). This water was used throughout the project. Prior to adhesion assays, *S. epidermidis* cells were stained by adding 2 µL of 3.34 mM SYTO 9, followed by a 15 min incubation period at room temperature in the dark. Staining was not required for *Ps. fluorescens* due to the mCherry fluorescence protein marker. Bacterial suspensions were then diluted in RW^{-C} to an OD of 0.2 for dynamic adhesion essays with and without flux constituting a feed concentration of approximately 10^7 CFU.mL^{-1}.

2.2. Microbial Adhesion to Solvents

The Microbial Adhesion to Solvents (MATS) assays were performed to assess the hydrophobic character and Lewis acid–base properties of the bacterial organisms used in this study. This method is based on the comparison between microbial cell surface affinity to a monopolar solvent and an apolar solvent which both exhibit similar Lifshitz-van der Waals surface tension components. The

MATS solvents used in this study were chloroform (an electron acceptor solvent), hexadecane (nonpolar solvent), ethyl acetate (an electron donor solvent), and decane (non-polar solvent) were of the highest purity grade (Sigma-Aldrich, Ireland). The experimental procedure was performed as described by Bellon-Fontaine et al. [38] with minor modifications. Briefly, bacterial cells were incubated to an OD_{600} of 1.0 and washed twice in RW^{-C} by centrifugation (Hettich, Germany) at 5000 RPM for 10 min. collected bacterial pellets were then suspended and diluted in RW^{-C} to an OD_{400} of 0.8. Individual bacterial suspensions (2.4 ml) were first mixed with 0.4 ml of the respective solvent and then mixed for 60 s using a Vortex mixer (Stuart, UK). The mixture was allowed to stand for 15 min to ensure complete separation of phases, after which 1 ml from the aqueous phase was carefully removed and its final optical density measured at OD_{400nm}. The percentage of adhesion of bacterial cells in the solvent phase was calculated using the following equation:

$$\%\ adherence = \left(\frac{A_o - A}{A_o}\right) \times 100 \qquad [1]$$

where A_o is the optical density of the bacterial suspension before mixing at OD_{400} and A is final optical density after mixing.

2.3. Bacterial Electrophoretic Mobility

Overnight bacterial cultures were harvested by centrifugation (5000 RPM, 10 mins) and washed twice with 0.001 M NaCl before diluting to an OD_{600} of 0.2. Separately, the pH of individual 0.001 M NaCl solutions was adjusted to pH 3, 7 and 9 by adding nitric acid or potassium hydroxide. Prior to electrophoretic mobility readings, the bacterial suspension was diluted to a hundredth in

the pre-prepared pH solutions suspension (2 mL final volume) which was then placed in a capillary cuvette that was placed in a Zetasizer instrument (Malvern Instruments, UK) for electrophoretic mobility measurements. Each experiment was performed in triplicate using three independent cultures.

2.4. Reverse Osmosis/Nanofilter Membranes

The thin film composite (TFC) polyamide membranes chosen for this experiment were NF270 (FilmTec Corp., USA) and BW30 (FilmTec Corp., USA). Coupons of BW30 and NF270 were rinsed and immersed in MilliQ water overnight prior to adhesion experiments and kept in the fridge. Samples for AFM roughness analysis were air dried after immersion.

2.5. Atomic Force Microscopy

Atomic Force Microscopy (AFM) was performed on membranes using a Nanowizard JPK Instruments (Berlin, Germany) for surface roughness and surface defect analysis. The topographical imaging was carried out with a scan rate of 0.4 Hz using a Silica Nitride cantilever with specified spring constant of 0.5 $N.m^{-1}$ and a resonant frequency between 50-65 Hz. The imaging programme Gwyddion [39] was used for image analysis. All images were taken in air at room temperature in tapping mode with the surface roughness measured at 10 µm x 10 µm and 50 µm x 50 µm. Surface roughness and average roughness were calculated using the equations provided by Gadelmawla et al. [40].

2.6. Adhesion Experiments

2.6.1. Dynamic initial adhesion assays in the absence of pressure

Initial adhesion assays were performed as described by Semião et al. [16] with slight modifications. Freshly cut selected membranes (2 x 3 cm) were immobilized onto glass slides (VWR, Dublin, Ireland) using double sided tape (3M, Scotch^{TM}, Ireland) and inserted in individual flow cells (Model BST 81, Biosurface Technologies Corporation, Bozeman, MT, USA) with modified channel dimensions of 2.35 mm depth, 13 mm width and 50 mm length. The dynamic adhesion system was composed of the flow cell device, a peristaltic pump (Watson-Marlow UK 323E) and a feed container (Falcon Tube VWR 40 mL) with the cells in suspension all connected with silicone tubing (VWR, Ireland) in a closed loop system. The flow cells are small continuous-flow systems with a glass viewing port that allowed for *in situ* observations by microscopy. After removing bubbles from the system, "zero point" images at the membrane's focal plane were recorded using an epi-fluorescence microscope (Olympus BX 51) and a 20x objective with a field of view of 1450 μm^2.

Adhesion experiments were initiated by recirculating bacterial cells at a volumetric flow rate of either 22.2 or 66.6 $mL.min^{-1}$. A flow rate of 22.2 $mL.min^{-1}$ corresponds to a velocity of 0.012 $m.s^{-1}$, a Re_{dh} of 26.7 and a shear rate of 0.030 s^{-1}. A flow rate of 66.6 $mL.min^{-1}$ corresponds to a velocity of 0.036 $m.s^{-1}$, a Re_{dh} of 80.3 and a shear rate of 0.092 s^{-1}. Shear rate was calculated as described below. Images were acquired 1 minute after initiating the bacterial assay and every 5 minutes for a total adhesion period of 30 minutes. Fluorescence emissions of adhered *Ps. fluorescens* and *S.*

epidermidis cells were acquired using the microscope's U-MNG or U-MWIB excitation/emission filter cube systems.

At the end of every adhesion assay, non-adhering cells were removed from the system by introducing 40 mL of RW^{-C} in a non-recirculating mode at the volumetric flow rate used during the adhesion experiment. Acquired images were processed using Image J ® to determine bacterial surface coverage over time. At the end of each adhesion experiment, membranes containing adhered cells were kept for qualitative assessment.

The initial adhesion kinetics of both *Ps. fluorescens* and *S. epidermidis* on NF270 and BW30 membranes was calculated using the following equation:

$$q(t) = q_{max} \cdot (1 - e^{-\beta t}) \quad (2)$$

Where $q(t)$ is the bacterial loading as a function of time (t), q_{max} the maximum cell loading and the accumulation factor β obtained by the exponential fit of the adhesion experimental data. The linear region of the obtained curve was used to calculate the rate of adhesion by using the following expression:

$$k_d = \frac{\theta(t)}{\Delta t} \cdot \frac{1}{C_0} \quad (3)$$

where k_d is the deposition rate of *Ps. fluorescens or S. epidermidis* on membranes, $\theta(t)$ the number of adhered cells over a time period Δt between two time points and C_0 the initial bacterial suspension feed concentration.

Shear stress was calculated using the following equation for wall shear rate [41]:

$$\sigma = \frac{3Q}{2(\frac{h_o}{2})^2 w_o} \quad (4)$$

Where Q is the volumetric flow rate ($m^3.s^{-1}$), h_o is the height of the rectangular channel (m) and w_o is the width of the rectangular channel (m). Shear stress is calculated by applying the following equation:

$$\tau_w = \eta\sigma \quad (5)$$

where η is the absolute viscosity ($kg.m^{-1}.s^{-1}$). Based on the experimental conditions used during the adhesion assays, shear stress were calculated at 0.031 $N.m^{-1}$ and 0.093 $N.m^{-1}$ for a volumetric flow rate of 22.2 $mL.min^{-1}$ and 66.6 $mL.min^{-1}$ respectively.

2.6.2. Dynamic adhesion essays under permeate flux conditions

Adhesion experiments under permeate flux conditions were performed in a cross-flow system as previously described [16], with some modifications shown in Figure 1.

Membranes were first compacted in the Membrane Fouling Simulators (MFS) at 12 bar pressure and a feed flow rate of 0.66 $L.min^{-1}$ for 18 hours. This flow rate corresponds to a velocity of 0.35 $m.s^{-1}$, a Re_{dh} of 579 and a shear rate of 2588 s^{-1}. Two MFS devices holding individual membranes were connected in parallel holding each either a NF 270 or a BW 30 membrane. The MFS devices were connected to a 10 L autoclavable feed tank (Carboy, Nalgene, VWR Ireland) and a high pressure pump (P400 from Hydra-Cell, UK). Temperature was monitored in the feed tank with a temperature indicator (Pt 100, Radionics, Ireland) and maintained at 20ºC ± 1ºC with a coil inside the tank connected to a temperature controlled water bath (MultiTemp III, Pharmacia Biotech, Ireland). A back pressure regulator (KPB1L0A415P20000, Swagelok, UK) allows the

pressurization of the system up to the required pressure. The pressure was monitored in both feed and retentate side of the membrane cells with two pressure transducers (PTX 7500, Druck, Radionics, Ireland). The feed flow was measured using a flow meter (OG2, Nixon Flowmeters, UK). Data logging was set-up allowing for data collection of membrane cells inlet and outlet pressure, feed flow rate and temperature (PicoLog 1000, PicoTechnology, Radionics, Ireland). The pure water permeate volume was measured using a 1000 mL graduated bottle. Water flux was measured by the mass of permeate after 2 minutes, this was repeated every half an hour until a steady water flux was obtained.

Adhesion experiments were conducted with compacted membrane using RW^{-C} at 8 bar. After 15 minutes (which allowed the system to reach equilibrium) conductivity measurements of the feed and permeate were recorded for each MFS device using a TetraCon 325 conductivity probe (WTW, Germany). The bacterial suspension was then added and allowed to recirculate for 30 minutes. The MFS cells were then removed from the system and membranes were cut and prepared as described in section 2.7.1.

2.7. Qualitative analysis of membranes following adhesion experiments.

2.7.1. Scanning electron microscopy

Membrane samples were prepared for Scanning Electron Microscopy (SEM) observation following experiments performed in both flow cell and cross-flow system. Briefly, membranes were removed from the MFS or flow cell devices while submerged under MilliQ water to prevent bubbles and sampled in mini-Petri dishes. Adhered cells were immersed in a solution of 2.5% Glutaraldehyde for 24 hours to preserve overall bacterial cell shape and structure. This was followed by a stepwise dehydration treatment by exposing fixated samples in MilliQ water with

increased ethanol-volumes (10%, 25%, 50%, 75%, 90% and 100%) between 5-10 minutes exposure per increment [42]. During dehydration, membrane samples were submerged at all times. The final step at 100% ethanol was performed for 10 minutes before the membrane sample was removed and allowed to dry at room temperature.

Surface topography and bacterial adhesion preference were examined with a dual beam field-emission scanning electron microscope (Hitachi Quanta 3D FEG Dual Beam FE-SEM). Samples were dehydrated and 1 cm x 1 cm coupons were cut from the centre of the flow cell membranes. Coupons were adhered to SEM stubs using a carbon adhesive and a Gold coater (Eimtach K575K) which applied a thin layer of gold at 30 mA for 2 minutes. Images were taken at an accelerating voltage of 5 kV, current of 5.92 pA and magnifications of 1200x were taken. Samples were analysed using Image J ® software.

Surface topographical heterogeneities, or surface defects in the present paper, are defined as microscale surface roughness irregularities characterised by their irregular and random contours ranging from freeform shapes to straight trench lines of different sizes and depths. Surface defect analysis was performed on acquired SEM micrographs using Image J® through a series of different thresholding steps after manually outlining shape contours defining areas of topographical differences [43, 44]. Thresholding was performed according to Ng et al. [44] using the MultiThreshold plugin feature of Image J®. Highlighted areas were then manually outlined using the Image J® freehand selection and area size was measured using the measure option in the Anaylze drop down menu. Additionally adhesion orientation of *Ps. fluorescens* images was analysed using Image J ® and statistical analysis was conducted as shown in section 2.8.

2.8 Statistical analyses

Analysis of variance (ANOVA) was used to determine the variation in the number of counted *Ps. fluorescens* or *S. epidermidis* cells per cm^2 onto different membrane types (NF270 and BW30) for different flow rates and permeate flux regimes. When needed, a one-way analysis of variance was performed to test the significance of the differences in membrane type, flow rates and permeate flux on bacterial adhesion. Sample sizes are provided in each relevant figure and table. Error bars are represented as standard error of mean. All analyses were performed using Tukey's test for pairwise comparisons assuming equal variance with MINITAB v15.1 (Minitab Inc., State college, PA). All tests were performed at a 5% significance level.

3. Results and Discussion

3.1. Microbial Adhesion to Solvents

The results for microbial adhesion to solvents for *Ps. fluorescens* and *S. epidermidis* are shown in Table 1 where adhesion properties are similar to the properties found in the literature [45, 46]. Both bacterial cells show a high affinity for the acidic solvent chloroform suggesting they have a strong electron donor character, compared to a low affinity with the electron donor solvent ethyl acetate. However, *Ps. fluorescens* shows a higher affinity to chloroform with a percentage adhesion of 90% compared to 72% adhesion of *S. epidermidis*. This suggests that *Ps. fluorescens* has stronger electron donor characteristics than *S. epidermidis.* Ps. *fluorescens* and *S. epidermidis* also show a low affinity for the nonpolar solvents hexadecane and decane, with *S. epidermidis* having the lowest affinity. This suggests that both bacterial cells are hydrophilic, with *Ps. fluorescens* being more hydrophilic than *S. epidermidis*.

3.2. Bacterial Electrophoretic mobility

The global surface charge of *Ps. fluorescens* and *S. epidermidis* cells were evaluated in this study as part of the characterization of the physicochemical properties of the cells. Electrophoretic mobility (EM) measurements were performed at pH values 3, 7 and 9 which are presented in Figure 2. All tested strains were electronegative and the values obtained are similar to those found in literature [47, 48] EM values reached their minimum at pH 7 with EM values of -1.48 and -1.7 (10^{-8} m^2/V.s) for both *Ps. fluorescens* and *S. epidermidis* cells respectively. As pH increases from 3 to 7, the global surface charge increased for both *Ps. fluorescens* and *S. epidermidis* cells as observed by the increasing negative EM. While cell wall electronegativity was stable for *Ps. fluorescens* cells at pH 7 and 9, the negative surface charge of *S. epidermidis* was reduced as observed by its decreasing negative EM from -1.7 to -1.4 µmcm/Vs at pH 7 and 9 respectively. As similarly shown by Tourney et al. [49], a deprotonation of cell wall functional groups takes place with increasing pH environments, which manifests itself with increasing EM, until all functional groups are fully deprotonated [47]. This difference in behaviour suggests that *Ps. fluorescens* and *S. epidermidis* cell wall properties are uniquely defined and that the observed EM variations between the two strains could be indicative of differences in cell wall composition, consequently manifesting in different adhesion behaviour.

3.3. Surface Roughness and Membrane Topographical heterogeneities

Surface characterization in terms of surface roughness was assessed through Atomic Force Microscopy (AFM) at three random areas of 10 µm x 10 µm for all tested membrane samples, as presented in Table 2. Additional Contact angle and Zeta Potential values were obtained from the

literature [50-52]. The mean surface roughness of BW30 and NF270 membranes were found to be in agreement with roughness values found elsewhere [53, 54]. Interestingly, roughness analyses from small and large scanned areas also indicated a significant variation in roughness measurements [15, 18, 19]. This variability in roughness values can be attributed to differences in membrane batches used during this study, but more importantly, from random areas selected for AFM scanning.

To test the latter hypothesis, a larger raster scanning area of 50 µm x 50 µm was used to first detect potential defect regions on membranes and secondly to establish the variation in roughness measurements caused by these surface defects. Representative AFM micrographs of small (10 µm x 10 µm) and large (50 µm x 50 µm) raster scanning areas performed on NF270 (A-C) and BW30 (B-D) membranes are presented in Figure 3. Large raster scans on membranes generally led to the detection of significant membrane topographical heterogeneities on both NF270 (C) and BW30 (D) that were otherwise missed in smaller raster scans (Figure 3 A-B).

Surface topographical heterogeneities were measured for their depth and width using AFM averaged over 10 different images. As shown in Table 3, the defect width was measured at 10 ± 2.2 µm with a depth of 1 ± 0.2 µm for the NF270 and 12 ± 1.6 µm with a depth of 0.4 ± 0.1 µm for the BW30. Although the width of topographical heterogeneities was similar for both membranes, each membrane provided a different adequate area for bacterial adhesion. The defect dimensions of NF270 membranes, 1 ± 0.2 µm in depth, closely match the size of both *Ps. fluorescens* and *S. epidermidis* with widths of approximately 1 µm, as described in section 2.1. This defect size could potentially accommodate both bacterial strains, protecting them from shear stress. In contrast, the BW30 defect depth of 0.4 ± 0.1 µm was found to be less than half of the

bacterial width, therefore preventing less shielding from shear stress which may be a less favourable adhesion site under dynamic flow conditions.

From the Contact Angle and Zeta Potential values presented in Table 2 both NF270 and BW30 membranes are hydrophilic and negatively charged. The contact angle is higher for the BW30 at 25.6˚ compared to a lower contact angle of 8.4˚ for the NF270. This indicates that the BW30 is slightly more hydrophobic compared to the NF270. The NF270 had a higher negative charge with a zeta potential of -24 mV compared to the BW30, which had a lower zeta potential of -5.2 mV. As the bacterial electrophoretic mobility was shown in the previous section to be negatively charged, the influence of a clean membrane surfaces' negative electrostatic charge could repel the bacteria causing a reduction in attachment [10] where the NF270 membrane could be expected to repel the cell more than the BW30 membrane.

3.4. Dynamic Initial Adhesion Assays

To assess the significance of membrane topographical heterogeneities on bacterial adhesion, experiments were performed at two different hydrodynamic conditions in the absence of permeate flux to qualitatively and quantitatively assess the adhesion of rod and cocci shaped model organisms in relation to the presence of membrane topographical heterogeneities.

Dynamic adhesion assays were performed onto NF270 and BW30 membranes at flow rates of 22.2 mL min^{-1} and 66.6 mL min^{-1} to establish whether cross-flow hydrodynamics had a significant impact on the initial adhesion of *Ps. fluorescens* and *S. epidermidis* cells. Maximum cell loading

(q_{max}) and adhesion velocity (k_d) shown in Table 4 were hence calculated from these results using Eq.1 and Eq.2 respectively.

The volumetric flow rates had no significant effect on the observed maximum cell loadings on membranes for both *Ps. fluorescens* (ANOVA, p=0.3463) or *S. epidermidis* (ANOVA, p=0.292), while the type of membrane was a determining factor during the adhesion of *Ps. fluorescens* cells (ANOVA, p=0.0001) but not for *S. epidermidis* (ANOVA, p= 1.00). In the case of *Ps. fluorescens,* a 20-fold increase in maximum cell loading was observed for rougher membranes (BW30) compared to flat membranes (NF 270). These results suggest that the difference in *Ps. fluorescens* and *S. epidermidis* surface physico-chemical properties as well as membrane surface properties may have influenced bacterial adhesion. The study by Margalit et al [55] has shown in a model of a parallel plate flow chamber that bacterial deposition can be influenced by the bacterial-surface interactions including bacterial dimensions, buoyancy and predisposition to adhere depending on the surface and bacteria used.

The accumulation of bacterial cells onto membranes following 30 minutes adhesion experiments at different flow rates are presented in Figure 4. Rough membrane surfaces (BW30) led to a 1 log increase of accumulated *Ps. fluorescens* cells (10^7 cells cm^{-2}) compared to the smoother NF 270 membrane (10^6 cells cm^{-2}) irrespective of volumetric flow conditions. This difference in adhesion profile could be influenced by differences in membrane properties. As previously discussed, the NF270 membrane is smoother, more hydrophilic and more negatively charged; hence bacterial adhesion to the NF270 membrane is expected to be lower compared to the BW30 membrane. Membrane surface properties, however, did not significantly affect the adhesion of *S. epidermidis* cells where deposition was found to be approximately 3 x 10^6 cells.cm^{-2} on both NF270 and BW30

membranes, irrespective of the flow rate conditions used during the experiment (ANOVA, p=1.0). These differences in bacterial attachment might therefore be influenced by bacterial properties rather than predominantly membrane properties, however further studies are required into bacteria-surface interactions.

In contrast to *S. epidermidis* cells, *Ps. fluorescens* possess flagella that may potentially contribute to surface adhesion onto rougher surfaces. Adhesion was significantly greater on the rougher BW30 membrane, which has more prominent surface features compared to NF270 membranes (ANOVA, p<0.0001) as previously discussed. The presence of these surface features may act as anchoring sites for *Ps. fluorescens* cells allowing them to withstand changes in flow conditions and therefore increase their adhesion as seen in Figure 4. The lack of prominent anchoring sites on the smoother NF270 membrane surface could explain the poor adhesion of *Ps. fluorescens* cells under hydrodynamic conditions. In a recent study, Friedlander et al. [56] showed that initial bacterial attachment to surfaces is improved by swimming motility and that the presence of flagella could improve access to surfaces as opposed to the presence of pili present in *Staphylococcus* cells which can only provide limited motility and adhesive properties [56].

3.5. Scanning Electron Microscopy

To qualitatively assess the significance of topographical heterogeneities on bacterial adhesion, SEM analyses were performed following dynamic adhesion assays of NF270 and BW30 membranes as described in section 3.1. The collected data was then used to determine the fraction of membrane defect surface area as well as the mean fraction of total adhered bacterial cells within defect areas for both *Ps. fluorescens* and *S. epidermidis* (Figure 5).

As can be seen in Figure 5, the defect area was found to be in the order of one tenth of the total membrane surface with averages of 7% and 12% of the total surface area of NF270 and BW30 membranes. BW30 was characterised by a higher fraction of 12% of defect areas compared to 7% for the NF270 (ANOVA, p= 0.025). Regardless of the adhesion conditions used, bacterial adhesion within topographical heterogeneities accounted for between 11% and 30% of the total bacterial counts on NF270 and BW30 respectively.

The number of adhered *S. epidermidis* cells within NF 270 membranes defect areas doubled from 15% to 30% when subjected to permeate flux conditions. No significant changes in adhesion were obtained for *Ps. fluorescens* when subjected to permeate flux for the NF270 membrane. On rougher BW30 membranes, however, permeate flux conditions led to a lower fraction of adhered *Ps. fluorescens* within membrane topographical heterogeneities as observed by a 2-fold reduction cell coverage within defect areas. In contrast, no significant changes were obtained for *S. epidermidis* when subjected to permeate flux.

When comparing the adhesion of cells within defects with and without the presence of permeate flux *Ps. Fluorescens* showed a higher level of adhesion within these surface defects under zero flux compared to that under flux conditions on the BW30 with NF270. The *S. epidermidis* however showed very little difference in adhesion on the BW30 with and without permeate flux conditions. These interactions between both the membrane and bacteria will require further research.

Considering that the observed topographical heterogeneities on both NF270 and BW30 were shown to be larger than the average bacterial dimensions (Table 3) the likelihood of a potential shielding effect of cells within these surface defects may contribute to a reduced detachment caused by weaker hydrodynamic shear forces. As previously discussed, certain topographies

created on substrates such as polymethyl methacrylate, silicone and stainless steel have been shown to promote bacterial adhesion [24-29]. Scheuerman et al. [57] noted that the edges of groves provided favourable areas for bacterial adhesion. This was later confirmed by Lee et al. [58] who showed that bacterial adhesion occurred in areas of low shear stress. Topographical heterogeneities on the membrane surface may provide areas of low shear stress therefore promoting adhesion within defect areas as shown in Figure 6, which shows SEM images of *Ps. fluorescens* and *S. epidermidis* cells adhered to both membranes in defect areas. This in turn may consequently serve as a protective niche in which bacterial cells may proliferate and form biofilms.

The angular orientation of adhered *Ps. fluorescens* with respect to the direction of flow was analysed to determine whether adhesion onto the surface of the membrane differs between defect areas and homogenous areas as can be seen in Figure 7. This analysis helped clarify whether cells adhering onto membranes and membrane surface defect areas follow a pattern based on flow direction or whether this adhesion was stochastic in nature (i.e. against the flow direction) due to shear stress shielding surface defects can provide.

It is hypothesized that the orientation of the bacteria adhered is dependent on physiochemical properties such as the presence of bacterial flagella [33, 55, 59, 60] for the adhesion of bacteria. It has also been suggested that bacterial properties such as flagella can assist in the orientation of adjacent bacterial cells during initial adhesion as previously described for particles and bacterial cells in other studies [10, 61, 62]. This could interfere with the adhesion orientation of the cells resulting in the random distribution in Figure 7.

From Figure 7 there is no noticeable difference in the angular orientation of adhered cells for both membranes with (Figure 7 E-F) and without permeate flux conditions (Figure 7 A-D). The

adhesion orientation of the bacterial cells appears to be randomly distributed as there was no difference in adhesion orientation between NF270 (Figure 7 A, C, E) and BW30 (Figure 7 B, D, F). As shown in the white bar section of Figure 7, the angular orientation of the bacterial cells within defects are also randomly distributed from 0-90˚. As previously discussed, this random distribution of adhered bacterial cells may be due to bacterial properties. These interactions, however, require further studies.

Conclusions

The effects of membrane surface topographical heterogeneities on the adhesion of *Ps. fluorescens* and *S. epidermidis* were investigated under no-flux and flux conditions using a combination of fluorescence microscopy AFM and SEM techniques. The characterized membranes' topographical heterogeneities were shown to be much larger than the dimensions of the tested cells, hence potentially providing low-shear areas in which adhered cells may accumulate. In the absence of permeate flux conditions, membrane properties such as roughness, hydrophobicity and surface charge as well as bacterial properties such as electrophoretic mobility, hydrophobicity and flagella/pili were shown to have a significant effect on adhesion. The fraction of bacteria adhered within surface defects were found to cover up to 30% surface area. This was higher than the fraction of defect areas which covered up to 13% surface area of the membrane. With the introduction of permeate flux conditions, the fraction of bacterial adhesion within topographical heterogeneities was found to depend on the bacteria and membrane properties. Moreover, cell angular orientations during adhesion under permeate flux suggests that the angle of attachment is determined by a stochastic process with no noticeable

difference between angle of attachment for defect areas and membrane surface. Membrane properties become an important feature in bacterial adhesion areas protecting topographical heterogeneities from hydrodynamic shear stress, these niches could potentially provide areas that promote biofilm growth. In full scale nanofiltration processes, however, the presence of a thin conditioning film on the membrane surface might mask the effect of these heterogeneities. Further studies are therefore needed to investigate this.

Acknowledgements

This work was supported by the European Research Council (ERC), under grant number 278530 and also with the financial support of Science Foundation Ireland under Grant number SFI 11/RFP.1/ENM/3145. The authors thank Dr. Ellen L. Lagendijk from the Institute of Biology Leiden, Netherlands for the gift of the *Pseudomonas fluorescens* PCL1701 strain. We thank Dr. Ian Reid of the NIMAC microscopy platform and Prof. Suzi Jarvis and the Nanoscale Function Group at UCD. We thank Dr Alan Casey of the Nanolab Research Centre at Focas Research Institute, Dublin Institute of Technology. We thank Mr. Pat O'Halloran for his invaluable technical assistance, and Mr. Liam Morris for the construction of the MFS devices.

References

[1] B. Cyna, G. Chagneau, G. Bablon, N. Tanghe, Two years of nanofiltration at the Mery-sur-Oise plant, France, Desalination, 147 (2002) 69-75.

[2] H.S. Vrouwenvelder, J.A.M. van Paassen, H.C. Folmer, J. Hofman, M.M. Nederlof, D. van der Kooij, Biofouling of membranes for drinking water production, Desalination, 118 (1998) 157-166.

[3] C. Tortajada, Water Management in Singapore, International Journal of Water Resources Development, 22 (2006) 227-240.

[4] H.C. Flemming, Reverse osmosis membrane biofouling, Experimental Thermal and Fluid Science, 14 (1997) 382-391.

[5] G. Cheng, Z. Zhang, S. Chen, J.D. Bryers, S. Jiang, Inhibition of bacterial adhesion and biofilm formation on zwitterionic surfaces, Biomaterials, 28 (2007) 4192-4199.

[6] J.S. Vrouwenvelder, J.A.M. van Paassen, J.M.C. van Agtmaal, M.C.M. van Loosdrecht, J.C. Kruithof, A critical flux to avoid biofouling of spiral wound nanofiltration and reverse osmosis membranes: Fact or fiction?, Journal of Membrane Science, 326 (2009) 36-44.

[7] M. Herzberg, M. Elimelech, Physiology and genetic traits of reverse osmosis membrane biofilms: a case study with Pseudomonas aeruginosa, ISME J, 2 (2007) 180-194.

[8] T.H. Chong, F.S. Wong, A.G. Fane, The effect of imposed flux on biofouling in reverse osmosis: Role of concentration polarisation and biofilm enhanced osmotic pressure phenomena, Journal of Membrane Science, 325 (2008) 840-850.

[9] W.S. Ang, S.Y. Lee, M. Elimelech, Chemical and physical aspects of cleaning of organic-fouled reverse osmosis membranes, Journal of Membrane Science, 272 (2006) 198-210.

[10] A. Subramani, E.M.V. Hoek, Direct observation of initial microbial deposition onto reverse osmosis and nanofiltration membranes, Journal of Membrane Science, 319 (2008) 111-125.

[11] H.C. Flemming, Biofouling in water systems - cases, causes and countermeasures, Applied Microbiology and Biotechnology, 59 (2002) 629-640.

[12] S.-T. Kang, A. Subramani, E.M.V. Hoek, M.A. Deshusses, M.R. Matsumoto, Direct observation of biofouling in cross-flow microfiltration: mechanisms of deposition and release, Journal of Membrane Science, 244 (2004) 151-165.

[13] W. Lee, C.H. Ahn, S. Hong, S. Kim, S. Lee, Y. Baek, J. Yoon, Evaluation of surface properties of reverse osmosis membranes on the initial biofouling stages under no filtration condition, Journal of Membrane Science, 351 (2010) 112-122.

[14] W.R. Bowen, A.S. Fenton, R.W. Lovitt, C.J. Wright, The measurement of Bacillus mycoides spore adhesion using atomic force microscopy, simple counting methods, and a spinning disk technique, Biotechnology and Bioengineering, 79 (2002) 170-179.

[15] K. Boussu, B. Van der Bruggen, A. Volodin, J. Snauwaert, C. Van Haesendonck, C. Vandecasteele, Roughness and hydrophobicity studies of nanofiltration membranes using different modes of AFM, Journal of Colloid and Interface Science, 286 (2005) 632-638.

[16] A.J.C. Semiao, O. Habimana, H. Cao, R. Heffernan, A. Safari, E. Casey, The importance of laboratory water quality for studying initial bacterial adhesion during NF filtration processes, Water Research, 47 (2013) 2909-2920.

[17] O. Habimana, A.J.C. Semiao, E. Casey, The role of cell-surface interactions in bacterial initial adhesion and consequent biofilm formation on nanofiltrationfreverse osmosis membranes, Journal of Membrane Science, 454 (2014) 82-96.

[18] K. Boussu, Y. Zhang, J. Cocquyt, P. Van der Meeren, A. Volodin, C. Van Haesendonck, J.A. Martens, B. Van der Bruggen, Characterization of polymeric nanofiltration membranes for systematic analysis of membrane performance, Journal of Membrane Science, 278 (2006) 418-427.

[19] D.J. Johnson, S.A. Al Malek, B.A.M. Al-Rashdi, N. Hilal, Atomic force microscopy of nanofiltration membranes: Effect of imaging mode and environment, Journal of Membrane Science, 389 (2012) 486-498.

[20] A.A. Myint, W. Lee, S. Mun, C.H. Ahn, S. Lee, J. Yoon, Influence of membrane surface properties on the behavior of initial bacterial adhesion and biofilm development onto nanofiltration membranes, Biofouling, 26 (2010) 313-321.

[21] R.J. Crawford, H.K. Webb, T. Vi Khanh, J. Hasan, E.P. Ivanova, Surface topographical factors influencing bacterial attachment, Advances in Colloid and Interface Science, 179 (2012) 142-149.

[22] E. Medilanski, K. Kaufmann, L.Y. Wick, O. Wanner, H. Harms, Influence of the surface topography of stainless steel on bacterial adhesion, Biofouling, 18 (2002) 193-203.

[23] R.D. Boyd, J. Verran, M.V. Jones, M. Bhakoo, Use of the atomic force microscope to determine the effect of substratum surface topography on bacterial adhesion, Langmuir, 18 (2002) 2343-2346.

[24] R.L. Taylor, J. Verran, G.C. Lees, A.J.P. Ward, The influence of substratum topography on bacterial adhesion to polymethyl methacrylate, Journal of Materials Science-Materials in Medicine, 9 (1998) 17-22.

[25] K.A. Whitehead, J. Verran, The effect of surface topography on the retention of microorganisms, Food and Bioproducts Processing, 84 (2006) 253-259.

[26] S.B.S. Ghayeni, P.J. Beatson, R.P. Schneider, A.G. Fane, Adhesion of waste water bacteria to reverse osmosis membranes, Journal of Membrane Science, 138 (1998) 29-42.

[27] K.A. Whitehead, J. Colligon, J. Verran, Retention of microbial cells in substratum surface features of micrometer and sub-micrometer dimensions, Colloids and Surfaces B-Biointerfaces, 41 (2005) 129-138.

[28] S. Perni, P. Prokopovich, Micropatterning with conical features can control bacterial adhesion on silicone, Soft Matter, 9 (2013) 1844-1851.

[29] S. Hou, H. Gu, C. Smith, D. Ren, Microtopographic Patterns Affect Escherichia coli Biofilm Formation on Poly(dimethylsiloxane) Surfaces, Langmuir, 27 (2011) 2686-2691.

[30] M. Darestani, T. Chilcott, H. Coster, Changing the microstructure of membranes using an intense electric field: Filtration performance, Journal of Membrane Science, 449 (2014) 158-168.

[31] S.H. Maruf, A.R. Greenberg, J. Pellegrino, Y. Ding, Fabrication and characterization of a surface-patterned thin film composite membrane, Journal of Membrane Science, 452 (2014) 11-19.

[32] J.R. Du, S. Peldszus, P.M. Huck, X. Feng, Modification of membrane surfaces via microswelling for fouling control in drinking water treatment, Journal of Membrane Science, 475 (2015) 488-495.

[33] H. Ivnitsky, I. Katz, D. Minz, G. Volvovic, E. Shimoni, E. Kesselman, R. Semiat, C.G. Dosoretz, Bacterial community composition and structure of biofilms developing on nanofiltration membranes applied to wastewater treatment, Water Research, 41 (2007) 3924-3935.

[34] H.-C. Flemming, J. Wingender, The biofilm matrix, Nature Reviews Microbiology, 8 (2010) 623-633.

[35] H. Wang, M. Sodagari, L.-K. Ju, B.-m.Z. Newby, Effects of shear on initial bacterial attachment in slow flowing systems, Colloids and Surfaces B-Biointerfaces, 109 (2013) 32-39.

[36] J.S. Baker, L.Y. Dudley, Biofouling in membrane systems — A review, Desalination, 118 (1998) 81-89.

[37] E.M. Vrijenhoek, S. Hong, M. Elimelech, Influence of membrane surface properties on initial rate of colloidal fouling of reverse osmosis and nanofiltration membranes, Journal of Membrane Science, 188 (2001) 115-128.

[38] M.N. Bellon-Fontaine, J. Rault, C.J. van Oss, Microbial adhesion to solvents: a novel method to determine the electron-donor/electron-acceptor or Lewis acid-base properties of microbial cells, Colloids and Surfaces B: Biointerfaces, 7 (1996) 47-53.

[39] D. Necas, P. Klapetek, Gwyddion: an open-source software for SPM data analysis, Central European Journal of Physics, 10 (2012) 181-188.

[40] E.S. Gadelmawla, M.M. Koura, T.M.A. Maksoud, I.M. Elewa, H.H. Soliman, Roughness parameters, Journal of Materials Processing Technology, 123 (2002) 133-145.

[41] H.J. Busscher, H.C. van der Mei, Microbial adhesion in flow displacement systems, Clinical Microbiology Reviews, 19 (2006) 127-+.

[42] M. Herzberg, M. Elimelech, Biofouling of reverse osmosis membranes: Role of biofilm-enhanced osmotic pressure, Journal of Membrane Science, 295 (2007) 11-20.

[43] D.-Y. Huang, C.-H. Wang, Optimal multi-level thresholding using a two-stage Otsu optimization approach, Pattern Recognition Letters, 30 (2009) 275-284.

[44] H.-F. Ng, Automatic thresholding for defect detection, Pattern Recognition Letters, 27 (2006) 1644-1649.

[45] J. Dostálková, V. Jirku, G. Procházková, L. Kriklavová, T. Lederer, T. Brányik, Cell Surface Determinants Important for Biofilm-Based Solid Substrate Degradation, Journal of Biomaterials and Nanobiotechnology, 2013 (2013).

[46] G. Lerebour, S. Cupferman, M. Bellon-Fontaine, Adhesion of Staphylococcus aureus and Staphylococcus epidermidis to the Episkin® reconstructed epidermis model and to an inert 304 stainless steel substrate, Journal of applied microbiology, 97 (2004) 7-16.

[47] P.J. Kiers, R. Bos, H.C. van der Mei, H.J. Busscher, The electrophoretic softness of the surface of Staphylococcus epidermidis cells grown in a liquid medium and on a solid agar, Microbiology, 147 (2001) 757-762.

[48] M. Van Loosdrecht, J. Lyklema, W. Norde, G. Schraa, A. Zehnder, Electrophoretic mobility and hydrophobicity as a measured to predict the initial steps of bacterial adhesion, Applied and Environmental Microbiology, 53 (1987) 1898-1901.

[49] J. Tourney, B.T. Ngwenya, The effect of ionic strength on the electrophoretic mobility and protonation constants of an EPS-producing bacterial strain, Journal of Colloid and Interface Science, 348 (2010) 348-354.

[50] A.J. Semião, O. Habimana, E. Casey, Bacterial adhesion onto nanofiltration and reverse osmosis membranes: Effect of permeate flux, Water Research, 63 (2014) 296-305.

[51] K.L. Tu, L.D. Nghiem, A.R. Chivas, Coupling effects of feed solution pH and ionic strength on the rejection of boron by NF/RO membranes, Chemical Engineering Journal, 168 (2011) 700-706.

[52] C.Y. Tang, Y.-N. Kwon, J.O. Leckie, Fouling of reverse osmosis and nanofiltration membranes by humic acid—effects of solution composition and hydrodynamic conditions, Journal of Membrane Science, 290 (2007) 86-94.

[53] E.M.V. Hoek, S. Bhattacharjee, M. Elimelech, Effect of membrane surface roughness on colloid-membrane DLVO interactions, Langmuir, 19 (2003) 4836-4847.

[54] M. Mänttäri, T. Pekuri, M. Nyström, NF270, a new membrane having promising characteristics and being suitable for treatment of dilute effluents from the paper industry, Journal of Membrane Science, 242 (2004) 107-116.

[55] E. Margalit, A. Leshansky, V. Freger, Modeling and analysis of hydrodynamic and physico-chemical effects in bacterial deposition on surfaces, Biofouling, 29 (2013) 977-989.

[56] R.S. Friedlander, H. Vlamakis, P. Kim, M. Khan, R. Kolter, J. Aizenberg, Bacterial flagella explore microscale hummocks and hollows to increase adhesion, Proceedings of the National Academy of Sciences of the United States of America, 110 (2013) 5624-5629.

[57] T.R. Scheuerman, A.K. Camper, M.A. Hamilton, Effects of substratum topography on bacterial adhesion, Journal of Colloid and Interface Science, 208 (1998) 23-33.

[58] Y.K. Lee, Y.-J. Won, J.H. Yoo, K.H. Ahn, C.-H. Lee, Flow analysis and fouling on the patterned membrane surface, Journal of Membrane Science, 427 (2013) 320-325.

[59] C. Diaz, P.L. Schilardi, P.C. dos Santos Claro, R.C. Salvarezza, M.A. Fernandez Lorenzo de Mele, Submicron Trenches Reduce the Pseudomonas fluorescens Colonization Rate on Solid Surfaces, Acs Applied Materials & Interfaces, 1 (2009) 136-143.

[60] C. Diaz, P.L. Schilardi, R.C. Salvarezza, M. Fernandez Lorenzo de Mele, Have flagella a preferred orientation during early stages of biofilm formation?: AFM study using patterned substrates, Colloids and Surfaces B-Biointerfaces, 82 (2011) 536-542.

[61] C. Diaz, R.C. Salvarezza, M.A. Fernandez Lorenzo de Mele, P.L. Schilardi, Organization of Pseudomonas fluorescens on Chemically Different Nano/Microstructured Surfaces, Acs Applied Materials & Interfaces, 2 (2010) 2530-2539.

[62] R.J. Gohari, W.J. Lau, T. Matsuura, A.F. Ismail, Effect of surface pattern formation on membrane fouling and its control in phase inversion process, Journal of Membrane Science, 446 (2013) 326-331.

Figures

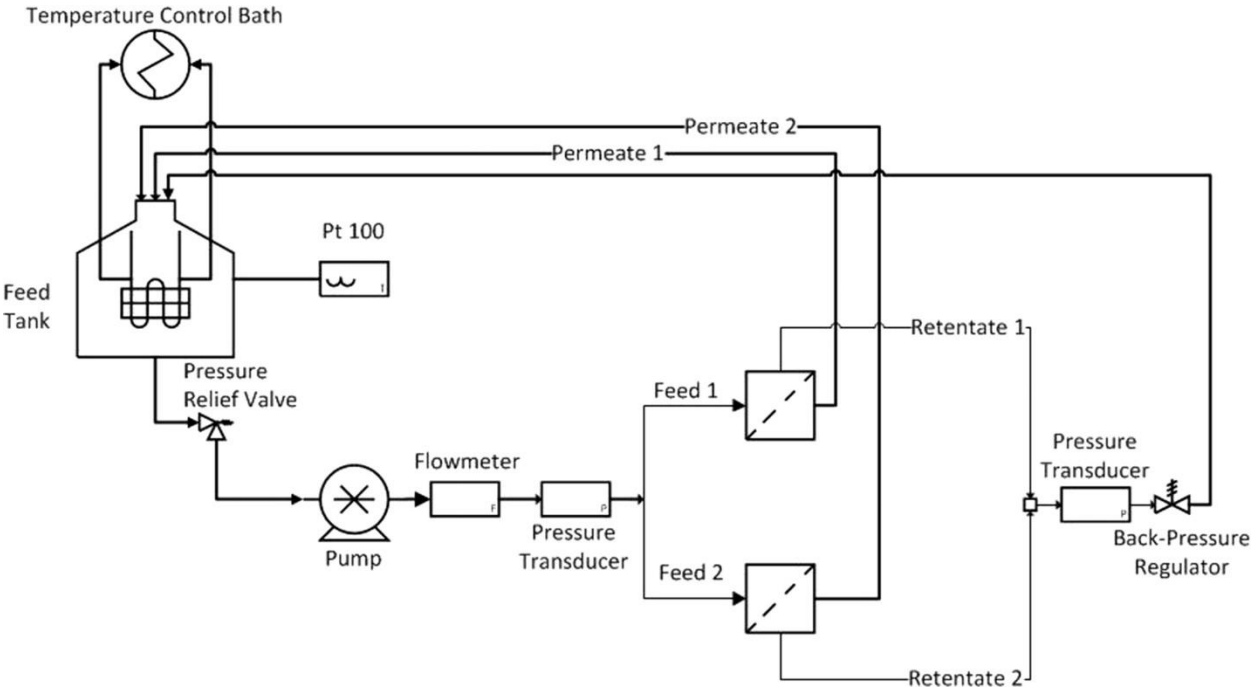

Figure 1. MFS Cross Flow System

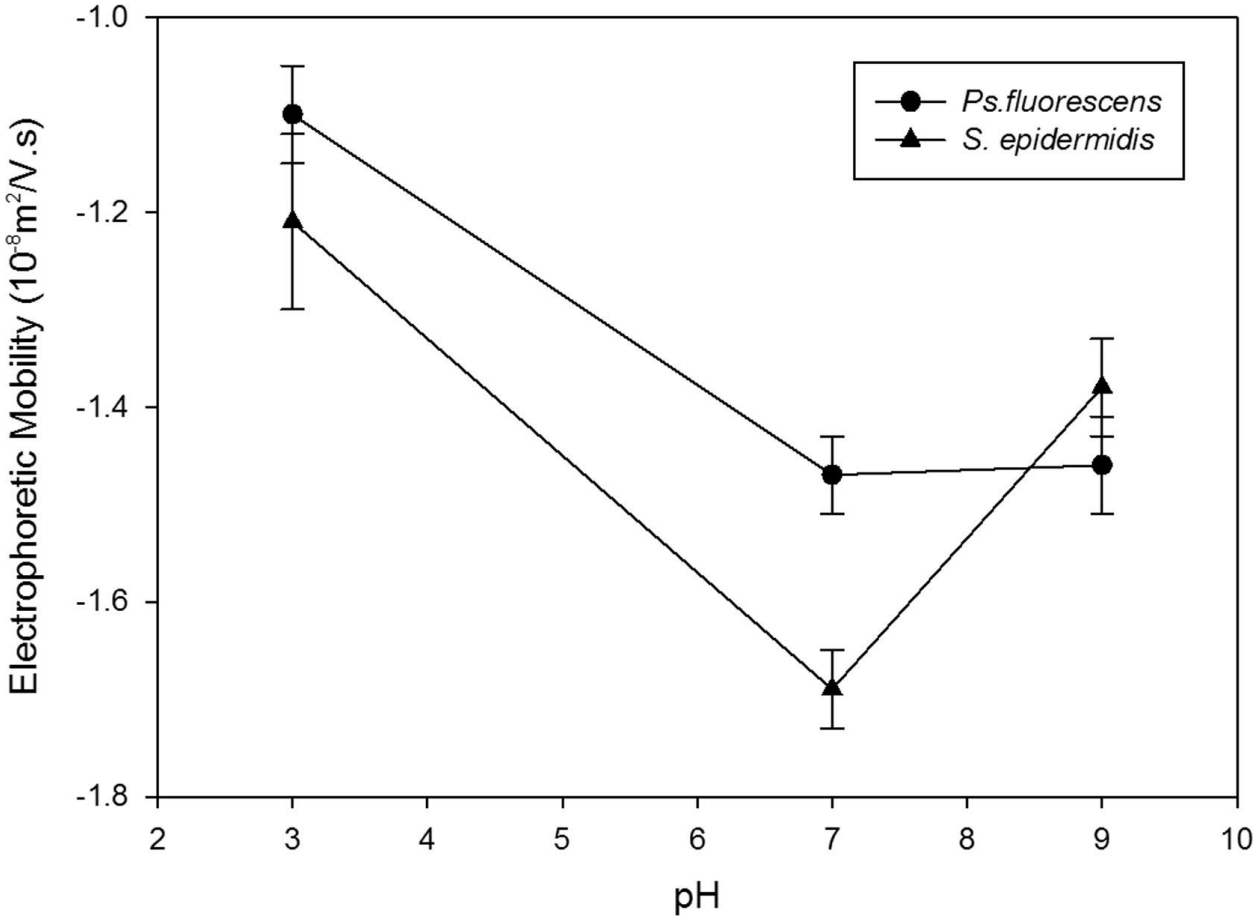

Figure 2: Electrophoretic mobility of *Ps. fluorescens* and *S. epidermidis.* Experiments were conducted in 0.001 M NaCl at pH 3, 7 and 9. Experiments were performed in triplicate and error bars represent standard error of mean.

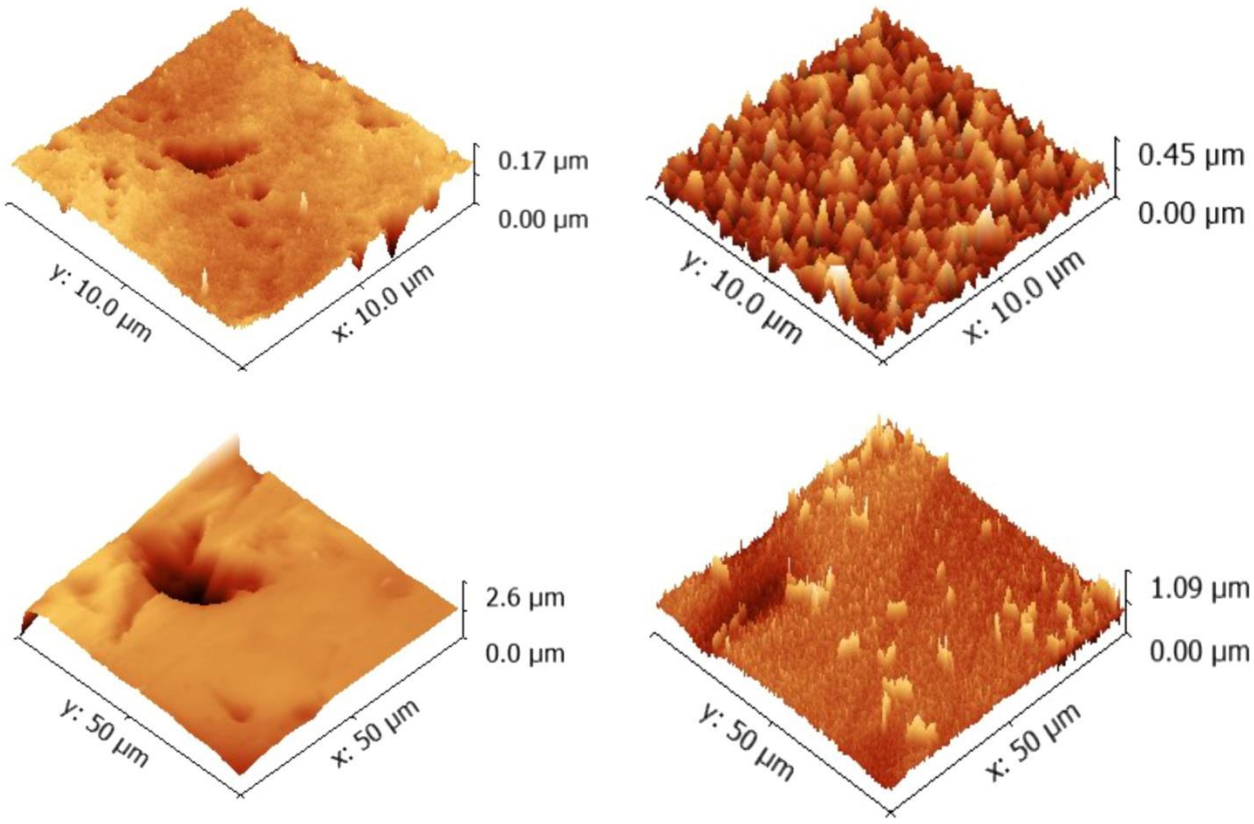

Figure 3: AFM images of NF270 (A) and BW30(B) with scanned areas of 10 µm x 10 µm and 50 µm x 50 µm for NF270(C) and BW30(D). Measurements were taken using tapping mode with a scan rate of 0.4 Hz using a Silica Nitride cantilever with specified spring constant of 0.5 N m^{-1} and a resonant frequency between 50-65 Hz.

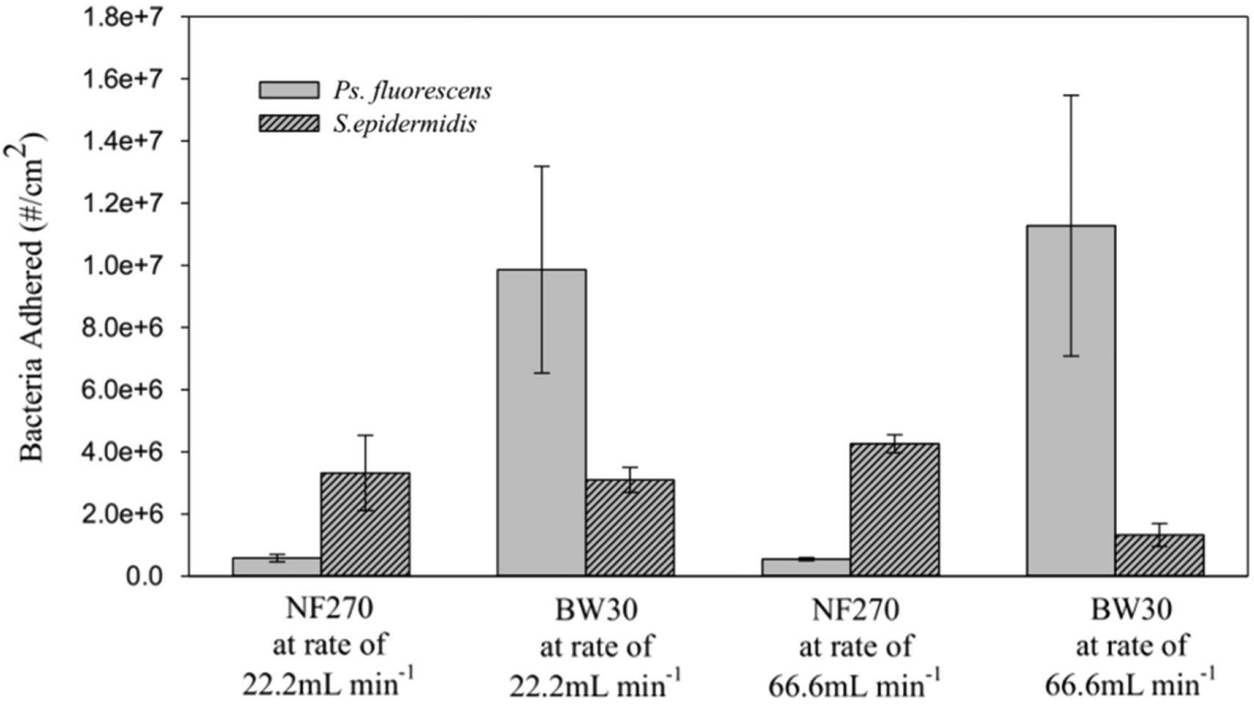

Figure 4: Observed adhered *Ps. fluorescens* and *S. epidermidis* cells on NF270 and BW30 membranes following 30 minutes adhesion experiments. Experiments were conducted in flow cells at flow rates set to 22.2 mL min^{-1} or 66.6 mL min^{-1} using bacterial suspensions of 10^7CFU mL^{-1}. Experiments were performed in triplicate and error bars represent standard error of mean. A flow rate of 22.2mL min^{-1} corresponds to a velocity of 0.012.m s^{-1}, a Re_{dh} of 26.7 and a shear rate of 0.030 s^{-1}. Also a flow rate of 66.6 mL min^{-1} corresponds to a velocity of 0.036.m s^{-1}, a Re_{dh} of 80.3 and a shear rate of 0.092 s^{-1}

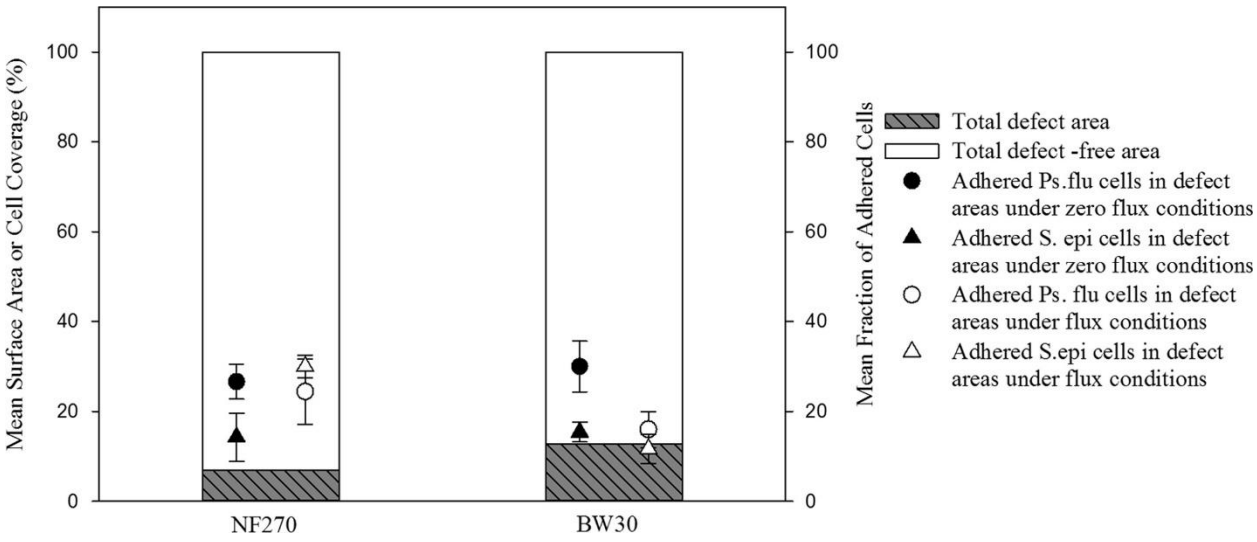

Figure 5: Surface area coverage (%) of *Ps. fluorescens* and *S. epidermidis* cells per cm^2 BW30 and NF270 membrane defect area. The mean surface area of topographical heterogeneities and microtopography irregularity-free areas are represented as shaded and white bars respectively. The fraction of adhered *Ps. fluorescens cells* (circle symbol) and *S. epidermidis* cells (triangle symbol) in membranes topographical heterogeneities under dynamic conditions (66.6 mL min^{-1}) are represented as closed (black symbols). The fraction of bacterial adhesion in membrane topographical heterogeneities under permeate flux conditions at 8 bar and 0.66 L.min^{-1} feed flow rate are symbolized with open (white) symbols. Experiments were performed in triplicate and error bars represent standard error of the mean.

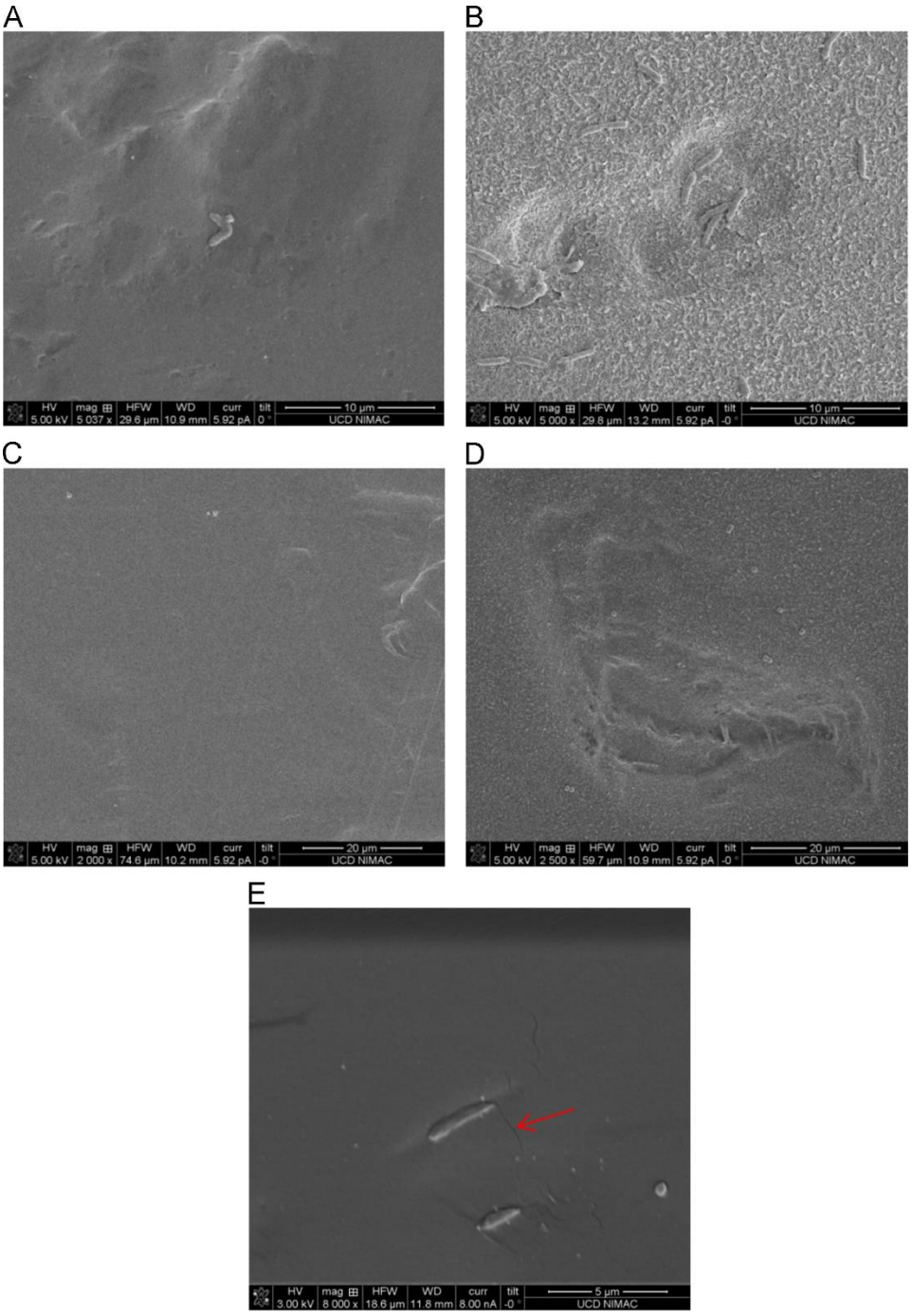

Figure 6: Representative SEM micrographs depicting the presence of bacterial cells within membrane surface topographical heterogeneities. Adhered *Ps. fluorescens* cells were observed on NF270 (A) and BW30 (B) membranes. Adhered *S. epidermidis* cells are depicted on NF270(C) and BW30 (D) membranes. Close-up micrograph portraying adhered Ps. *fluorescens* cells with their flagellum on a NF 270 membrane. Adhesion experiments were performed under cross flow with no permeate flux.

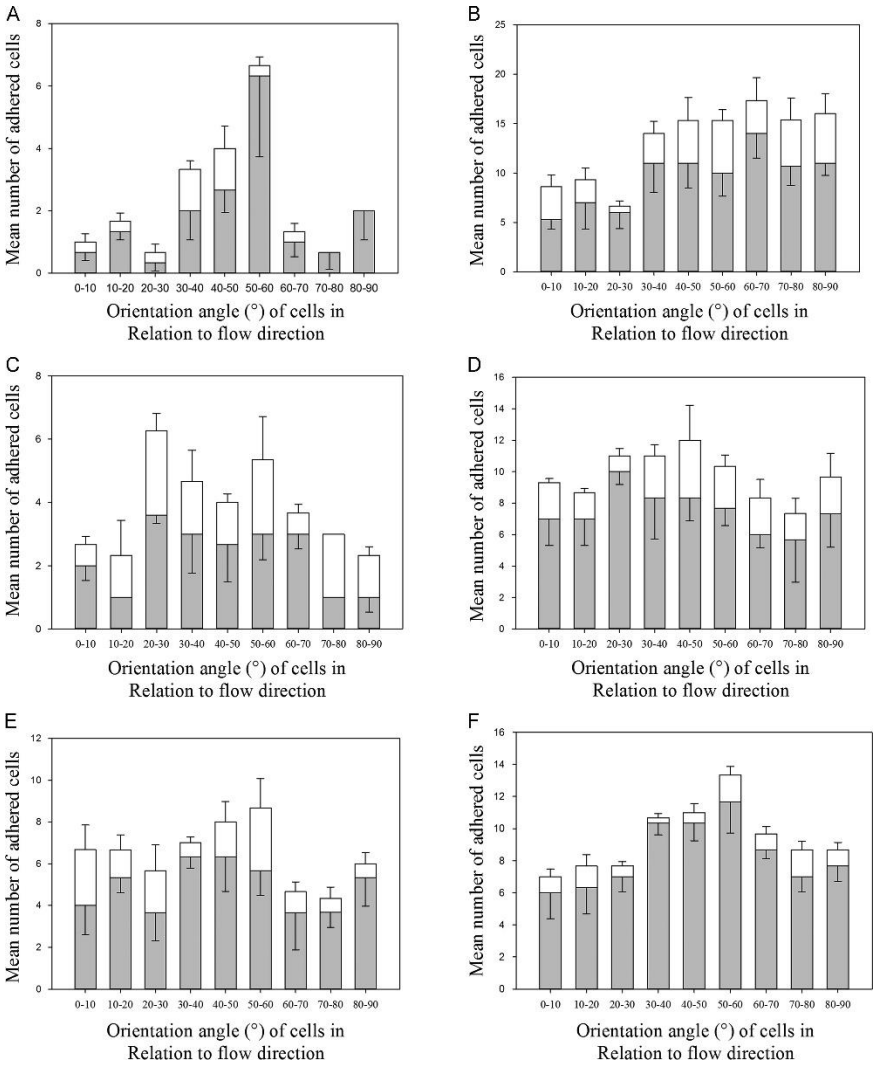

Figure 7: Population distribution of the mean number of adhered *Ps. fluorescens* cells, based on the angle at which they adhere on the membrane in relation to the direction of the flow. Each histogram is an accumulation of 5 random images. The angle of bacteria adhered to membrane without topographical heterogeneities (white) and angle of bacteria within topographical heterogeneities (grey), the accumulated white and grey areas are the total number of bacteria adhered to the membrane surface. The effect of volumetric flow velocities on the angle of adhesion were compared for NF270 (A, C, E) and BW30 membranes (B, D, F) at flow rates of 22.2 mL min^{-1} (A-B) and 66.6 mL min^{-1} (C-D) and under permeate flux (E-F). The effect of pressure on the angle of adhesion was compared for NF270 (E) and BW30 (F) under permeate flux conditions of 0.44Lmin^{-1} at 8 bar. Experiments conducted using flow cells were without pressure at room temperature and a cell concentration of 10^7 CFU mL^{-1}. A flow rate of 22.2mL min^{-1} corresponds to a velocity of 0.012.m s^{-1}, a Re_{dh} of 26.7 and a shear rate of 0.030 s^{-1}. Also a flow rate of 66.6 mL min^{-1} corresponds to a velocity of 0.036.m s^{-1}, a Re_{dh} of 80.3 and a shear rate of 0.092 s^{-1}

Table 1 – Affinity of *Ps. fluorescens* and *S. epidermidis* suspended in RW^{-C} for the four solvents used in the MATS analysis.

	%Adhesion			
	Chloroform	Hexadecane	Decane	Ethyl Acetate
Ps. fluorescens	90.20 ± 1.53	44.89 ± 3.67	67.56 ± 2.31	5.77 ± 0.39
S. epidermidis	71.96 ± 4.08	32.07 ± 4.91	49.25 ± 5.60	10.66 ± 2.53

Table 2 - Mean Roughness, Contact Angle and Zeta Potential measurements for BW30 and NF270 with scan areas of 10 µm x 10 µm. Error is represented using Standard Error of the Mean.

	R_A(nm)	R_{MS}(nm)	Contact Angle (°)	Zeta Potential (mV)
NF270	16.9 ± 4.94	23.67 ± 5.8	8.4 ± 0.5[a]	–24[b]
BW30	42.3 ± 5.5	53.9 ± 7.1	25.6 ± 0.8[a]	-5.2[c]

[a] Values from Semião et al (2014) [50]

[b] Values from Tu et al (2011) [51]

[c] Values from Tang et al (2007) [52]

Table 3 – Defect size characterisation in terms of width (μm), depth (μm) and maximum height (nm) for BW30 and NF270 membranes following AFM scanning area rasters of 50 μm x 50 μm averaged from 10 different images. Errors are represented as standard error of the mean.

	Defect Width (μm)	Defect Depth (μm)	Membrane Maximum Height (nm)
NF270	10 ± 2.2	1 ± 0.2	517.1± 98.6
BW30	12 ± 1.6	0.4 ± 0.1	342.5 ± 59.1

Table 4 – Estimated maximum cell loading and deposition rate of *Ps. fluorescens* and *S. epidermidis* on NF270 and BW30 under 22.2 mL min^{-1} and 66.6 mL min^{-1} volumetric flow rate conditions. Errors are represented as standard error of the mean. Experiments were repeated 3 times. A flow rate of 22.2mL min^{-1} corresponds to a velocity of 0.012.m s^{-1}, a Re_{dh} of 26.7 and a shear rate of 0.030 s^{-1}. Also a flow rate of 66.6 mL min^{-1} corresponds to a velocity of 0.036.m s^{-1}, a Re_{dh} of 80.3 and a shear rate of 0.092 s^{-1}

	Estimated Maximum cell loading q_{max} (10^7 cells cm^{-2})		**Adhesion Velocity k_d (10^{-3} cm min^{-1})**	
	22.2 mL min^{-1}	66.6 mL min^{-1}	22.2 mL min^{-1}	66.6 mL min^{-1}
***Ps. fluorescens* NF270**	0.17 ± 0.08	0.22 ± 0.03	0.17 ± 0.02	0.18 ± 0.02
***Ps. fluorescens* BW30**	3.36 ± 1.5	2.79 ± 1.35	3 ± 0.6	3.4 ± 0.6
***S. epidermidis* NF270**	0.57 ± 0.05	0.84 ± 0.06	1.05 ± 0.11	1.37 ± 0.12
***S. epidermidis* BW30**	0.46 ± 0.05	0.18 ± 0.03	0.93 ± 0.11	0.5 ± 0.1